THE JOURNAL OF PHYSICAL CHEMISTRY LETTERS
A JOURNAL OF THE AMERICAN CHEMICAL SOCIETY

pubs.acs.org/JPCL
Letter

Strong Second Harmonic Generation and Nonlinear Optical Activity in Chiral Supramolecular Polymers

Carlos H. D. dos Santos, Marcelo G. Vivas, Filipe A. Couto, Guy Koeckelberghs, Cleber R. Mendonça, and Leonardo De Boni*

Cite This: J. Phys. Chem. Lett. 2025, 16, 13007−13015

ABSTRACT: The growing demand for advanced optical materials has made nonlinear photonics a key area of research, particularly for developing new technologies. Therefore, this study focuses on chiral supramolecular structures, which are highly promising due to their exceptional second-order optical susceptibility ($\chi^{(2)}$) values. In particular, we investigated the origin and optical activity of second harmonic generation (SHG) in chiral polybinaphthalenes using femtosecond laser pulses. Our outcomes reveal a high $\chi^{(2)}$ value, up to 7 pm/V, influenced by the attached chromophores at the polymer backbone. Structural analysis showed rodlike/helical structures that promote directional preference for the SHG signal. Simulations unveil that the SHG process is connected to the quasi-phase matching process, and the material's robust chiral structure leads to high optical activity observed via lock-in amplifier detection. In conclusion, the conjunction of high SHG values and optical activity of these supramolecular structures makes them excellent candidates for chiral photonics applications.

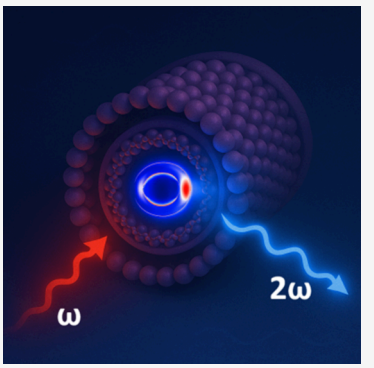

Chiral functionalized polymers have garnered particular interest, due to their straightforward capacity to conceive noncentrosymmetric supramolecular structures with high nonlinear polarizabilities.[1−5] This performance renders them outstanding candidates for applications involving second-order nonlinear optical (NLO) responses such as frequency conversion,[6] optical storage devices,[7,8] and electro-optic devices,[9,10] and the new field of chiral photonics.[11,12] Over the past few decades, significant efforts have been directed toward investigating and progressing on enhancing the NLO response at supramolecular systems, and notable evolution has been accomplished in the structure−property relationships, especially in periodically poled polymers (PPP).[13−15] The introduction of the suitable isolation group[16] (SIG) concept has been responsible for a pioneering design, e.g., spherical,[17] H-shaped,[18] star-type,[19] and hyperbranched,[20] that enhances the signal of second harmonic generation (SHG). On the other hand, synthesizing these supramolecular geometries requires complex and high-cost chemistry. The fabrication of PPP involves meticulous steps, including elevated temperatures and an intensive external electrical field. Besides, NLO chromophores attached to backbone polymers generally have a D-π-A (donor/acceptor) structure and typically exhibit a rodlike structure, leading to robust intermolecular dipole−dipole interactions within the supramolecular system. This characteristic significantly complicates the alignment of chromophores into a noncentrosymmetric arrangement induced by the poling process.[21,22] In addition, experimental measurements in colloidal systems using the SHG technique[23] allow us to determine the magnitude of the frequency upconversion in organic molecules,[24−27] as well as nanocrystal and bulk semiconductors (NCs).[28−31] Few studies reported SHG in supramolecular systems.[32] In this context, recognizing the significance of performing the nonlinear optical properties of the supramolecular materials, herein, we conducted a novel study of frequency-resolved second-order nonlinearities in novel samples of chiral donor-embedded polybinaphthalenes (CDEP) in dimethyl sulfoxide (DMSO) solution. In general, this class of polymer has a noncentrosymmetric twisted and rigid structure, such as a rodlike helical structure. The chirality and the chromophores are introduced to promote the increase in the nonlinear optical response and add new optical phenomena, as demonstrated by critical results in the literature.[33,34] In particular, chirality plays a fundamental role in SHG imaging[35−38] due to the selectivity of the circularly polarized pump light[39] and is crucial to providing information about the morphology and three-dimensional orientation of the molecules, including sensors and quantum optics applications.[39−42]

With this in mind, we present a SHG and optical activity frequency-resolved experimental study using a tunable femtosecond amplified pulsed laser. Atomic force microscopy (AFM) and dynamic light scattering (DLS) were also

Received: August 11, 2025
Revised: November 18, 2025
Accepted: November 26, 2025
Published: December 11, 2025

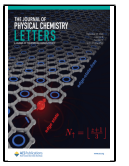

https://doi.org/10.1021/acs.jpclett.5c02495
J. Phys. Chem. Lett. 2025, 16, 13007−13015

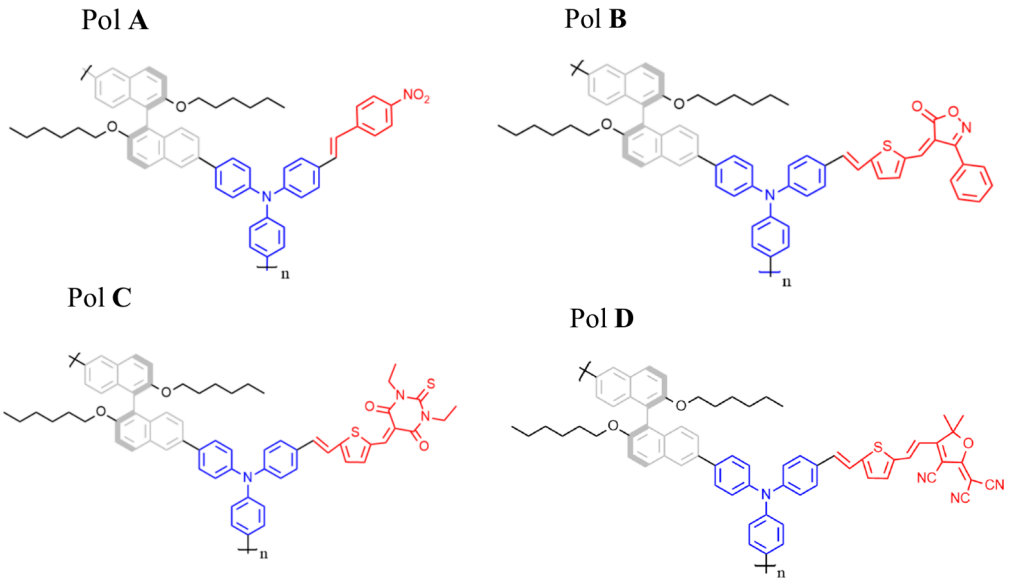

Figure 1. Supramolecular structure of chiral chromophore-functionalized polybinaphthalenes.

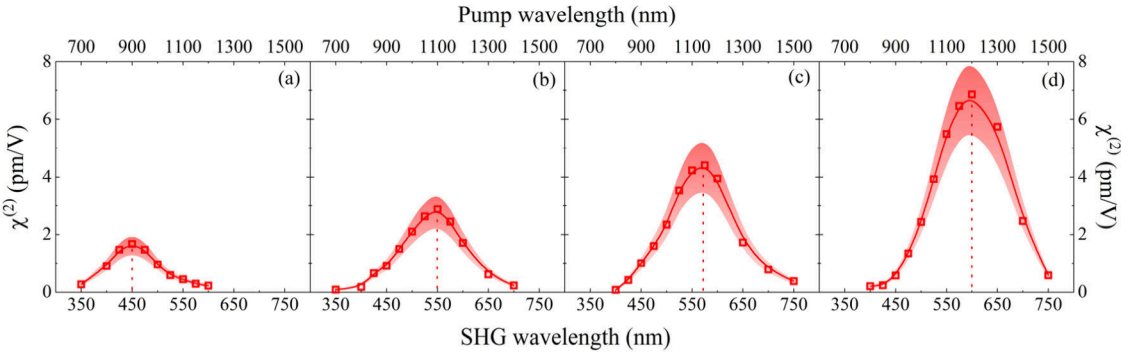

Figure 2. Symbols represent the dispersion of the second-harmonic generation ($\chi^{(2)}$) in pm/V units for the CDEP polymers in DMSO solution obtained by the SHG femtosecond technique: (a) A, (b) B, (c) C and (d) D. The solid line is present only to guide the eye.

employed to untangle structural information on polymers in solid-state and solution, respectively, such as the size and shape of the CDEP. AFM images unveil that the polymers present a hollow cylinder structure with a diameter of hundreds of nanometers, which agrees with the measures of DLS in the solution. Polarization studies performed in solution reveal the macroscopic contribution of the collected signal. Our results suggest that the fundamental origin of SHG may be attributed to quasi-phase matching (QPM) provided by finite-difference time-domain (FDTD) simulations to the helical supramolecular self-assembly, such as PPP systems, enhanced by quantum and classical mechanisms. Finally, the chirality is unveiled through optical activity SHG measurements, such as the difference between left and right polarization intensities, can reach up to 9%.

Figure 1 displays the molecular structure of the chiral supramolecular polymers, based on a triphenylamine group as a core (blue) linked to the two-chiral binaphthalene (S enantiomer) units in gray and functionalized chromophores, represented by red color, as can be seen in Figure 1. The details of the synthesis and linear circular dichroism measurements are described in ref 43. The main difference between the polymers is the functionalized chromophore with distinct electron-withdrawing groups (EWGs) responsible for triggering nonlinearities.

It is worth mentioning that $\chi^{(2)} \propto N\mu\beta E$, in which N is the concentration of chromophore, μ the dipole moment, β the first-order hyperpolarizability coefficient, and E the applied electric field. In this case, it implies that the $\chi^{(2)}$ signal can be increased using chromophores with higher hyperpolarizabilities and dipole moments or increasing the loading densities. Besides, the attachment of the chromophores as a side chain results in a treelike structure that prevents the undesired centrosymmetrical ordering of the chromophores, but becomes flexible enough to induce the noncentrosymmetry by electrical poling.[44] The absorption spectra presented in Figure SI-1 of the Supporting Information (SI) show two main one-photon absorption (1PA) bands at the UV-Vis region for all four polymers dissolved in DMSO solvent. The higher energy absorption band is found at all polymers centered around 350 nm, which is related to the binaphthalene core[44] and the lowest energy one (LE) to the triphenylamine core attached at chromophores A, B, C, and D centered, respectively, at 433, 545, 561, and 598 nm. No fluorescence at all was observed.

The microscopic dispersion of SHG observed in the Pol A, Pol B, Pol C, and Pol D in DMSO solution is depicted in Figure 2. In Figure SI-2(a), the quadratic dependence of the SHG with the laser intensity is displayed as an example for Pol A at an excitation wavelength of 1200 nm for six different concentrations. Also, in the Figure SI-2(b) (correct is Figure

https://doi.org/10.1021/acs.jpclett.5c02495
J. Phys. Chem. Lett. 2025, 16, 13007−13015

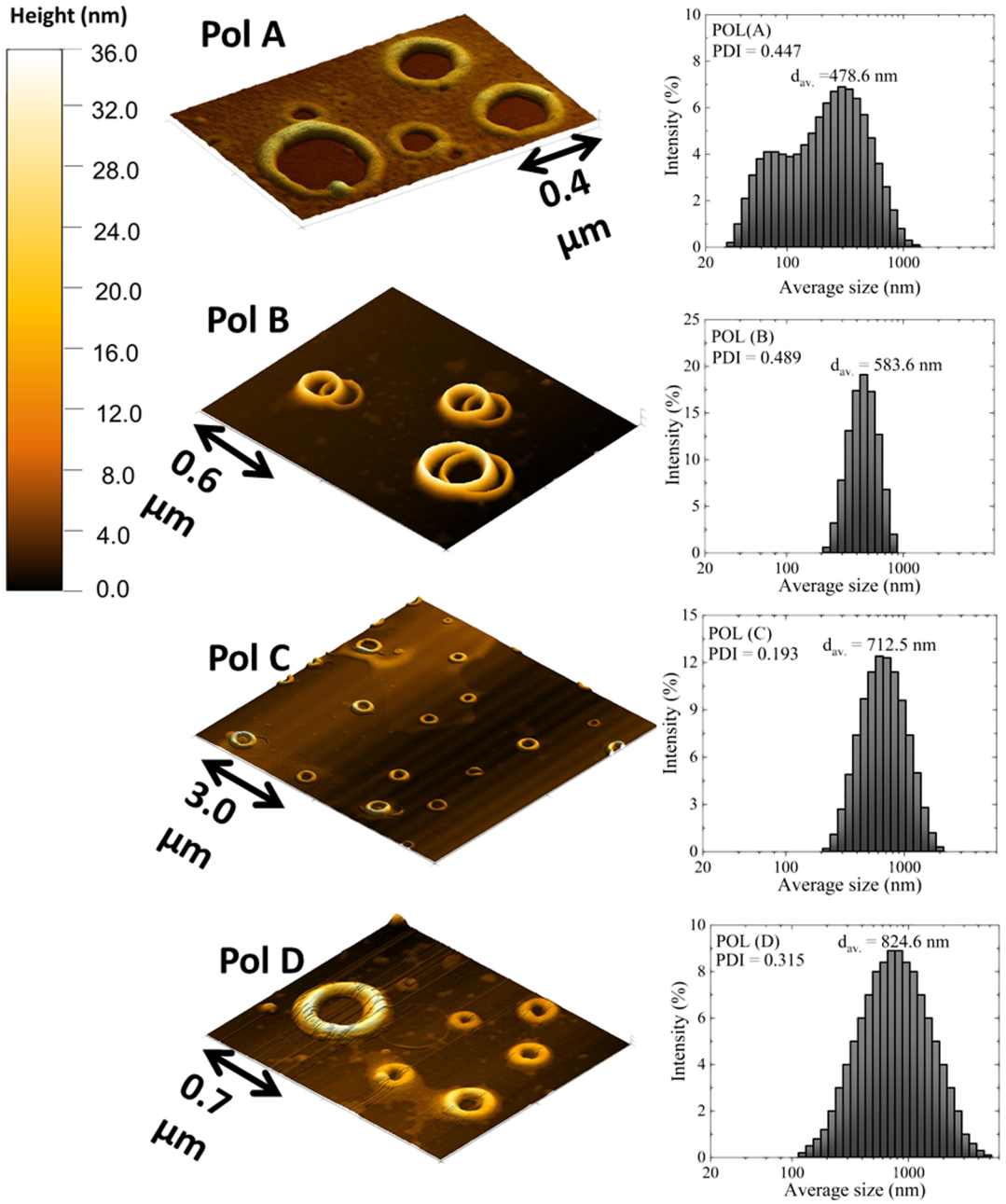

Figure 3. (Left) AFM topography images for CDEP polymers. (Right) Size distribution of the supramolecular structure of the polymers, as obtained from DLS data.

SI-2(e)), the SH signal is compared to a small standard molecule (*para*-nitroaniline) in order to quantify its value. Additionally, a previous analysis was performed to confirm whether the double-frequency signal detection has a microscopic or macroscopic derivation. In the SHG experimental setup, a broadband polarizer was placed before the photomultiplier (PMT) for s- and p-polarized detection. The result shows the same signal for both s- and p-polarization, which indicates a macroscopic origin (χ^2).

The χ^2 dispersion behavior is similar for all samples, in which the values tend to decrease for shorter and longer wavelengths concerning the peak (Pol A = 1.5 ± 0.4 pm/V at 900 nm, Pol B = 2.5 ± 0.7 pm/V at 1100 nm, Pol C = 4.5 ± 1.3 pm/V at 1150 nm, and Pol D = 7.1 ± 2.2 pm/V at 1200 nm). Initially, the high χ^2 peak values could be attributed to the two-photon absorption (2PA) transition in the near-infrared region,[44] which promotes enhancement in the SHG signal due to the two-photon resonance, which is described by the second-order time-dependent perturbation theory.[26] However, these polymers present a moderate 2PA cross-section, compared to other π-conjugated polymers. At the same time, the variance in the SHG maxima, reaching up to 5-fold when comparing Pol A with Pol D, cannot be explained only by considering the 2PA. Another effect would be the different spectral positions of 2PA bands among the polymers,[45,46] which could favor a resonance enhancement effect on the SHG signal. To understand this, a two-level model (2LM)[47] simulation for the LE absorption band (chromophore absorption band) was employed to calculate the 2PA enhancement factor that relates to the enhancement

https://doi.org/10.1021/acs.jpclett.5c02495
J. Phys. Chem. Lett. 2025, 16, 13007−13015

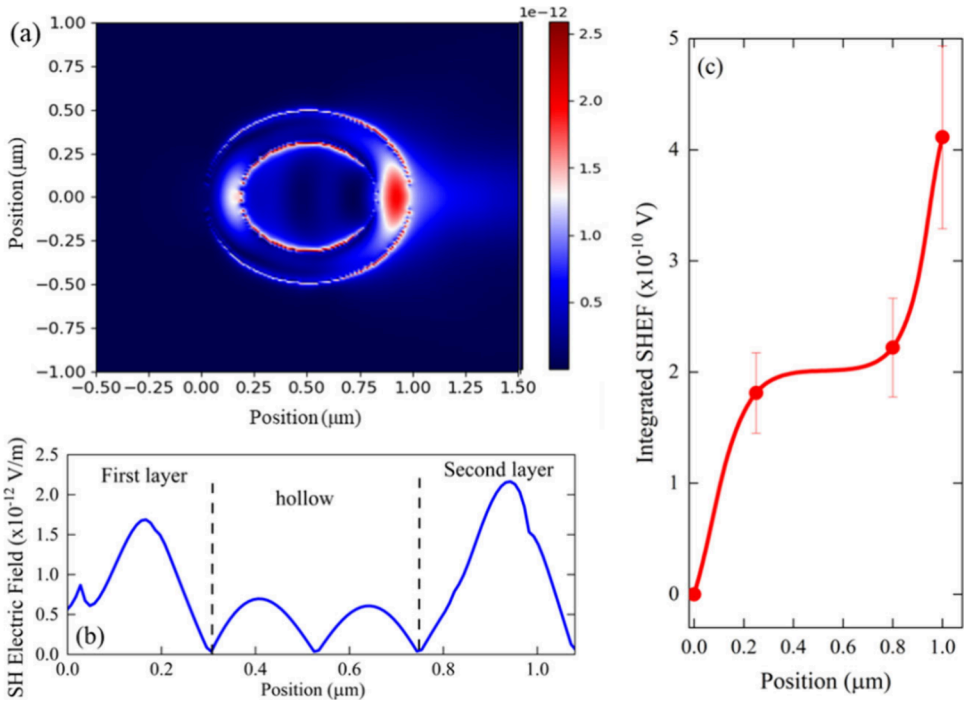

Figure 4. Simulation of the SH optical field generation for the Pol D at a pumping wavelength of 1200 nm. Panel (a) illustrates a color map of the magnitude of the SH electric field as a function of the position of the structure. Panel (b) is a cut in the $y = 0$ plane, showing the oscillation of the field. Panel (c) corresponds to the accumulated magnitude of the SH electric field throughout the structure, divided into sections, where the circles in red are the values of the integral in each section and the continuous line in red shows the trend of the values. The acronym SHEF stands for second harmonic electric field.

of SHG when the frequency of the scattered photon (2ω) is close to the 2PA allowed transition.[48] Using the second-order perturbation theory, we can clearly see this effect because the denominator in the dynamical term for 2LM is proportional to $(\omega_{01} - 2\omega)$, in which ω_{01} is the two-photon allowed transition frequency of chromophore (see the SI). As shown in Figure SI-2 (correct is Figure SI-3), similar results for the enhancement factor were found among the polymers, which suggests that the structural effect of polymers plays a fundamental role in the strong SHG signal observed. The curves of the 2PA enhancement factor are depicted in Figure SI-3 and are calculated by using eq SI-1, as shown in the SI. In this context, one alternative explanation for the χ^2 variances was to consider the polymer's size and shape combined with the 2PA effect. First, dynamic light scattering (DLS) and atomic force microscopy (AFM) measurements were performed to provide the geometrical characteristics of polymers in solution and solid state, respectively. A brief description of both procedures can be found in sections S4 and S5 of the SI. Figure 3 (left) shows the AFM topography images of the supramolecular structure of the CDEP polymers on the silicon substrate. The AFM images reveal a hollow cylindrical structure across all polymers, with similar cylinder wall thicknesses of 170 ± 40 nm, average heights of 32 ± 9 nm, and diameters ranging from 400 nm to 800 nm. In Figure 3 (right), we depict the size distribution (cylinder diameter) obtained from the DLS technique. First of all, a good agreement was found when we compared the cylinder diameter obtained from the AFM (solid-state) and DLS (in solution). Such an interesting outcome indicates that the polymers present a geometry similar in the solid-state and solution. As can be seen in DLS measurements, the average size of the size distribution presents a progressive increase, going from 478 nm (Pol A) to 825 nm (Pol D), with an average polydispersity index (PDI) value around 0.3, indicating a considerable level of polydispersity. In general, if PDI > 0.5, the distribution is rather broad and could significantly increase in the linear scattering in solution, which could affect the SHG conversion and consequently the optical activity signal in studied samples.[49].

By leveraging the findings of the structural dimensions of the polymers, a more comprehensive analysis was undertaken to understand the correlation between structure, size, and the origin of SHG. The peak values of χ^2 are plotted as a function of the respective volumes for CDEP structures, and a quadratic tendency is observed in Figure SI-4. The nonlinear optical effect generally has a linear dependence on the volume in nanomaterials.[50,51] This uncommon behavior indicates that it is not just a discrete effect concerning the increase in the structure size. On the other hand, a surface-to-volume analysis shows a minor surface contribution to larger structures, indicating the presence of additional SHG channels beyond symmetry breaking at the interface. As shown in AFM images, all the samples present a structure size in the SHG wavelength dimensions, in which a Quasi-Phase Matching (QPM) process may occur and amplify the nonlinear signal. On the other hand, phase matching happens predominantly in nonlinear optical crystals, where the refraction index for the pump and SHG frequency must be the same ($n_\omega = n_{2\omega}$) in a broad spectral region, which is not observed in our case. Elshocht et al.[52] demonstrated that chirality can act as a QPM process, due to the alternation of signals between the enantiomers in Langmuir−Blodgett films of a chiral polymer derived from helicenoquinone. In this case, these results allow us to obtain high $\chi^{(2)}$ values without the need to carry out the additional process of inverting second-order nonlinear optical susceptibility values, such as in the polling technique. This periodic

https://doi.org/10.1021/acs.jpclett.5c02495
J. Phys. Chem. Lett. 2025, 16, 13007−13015

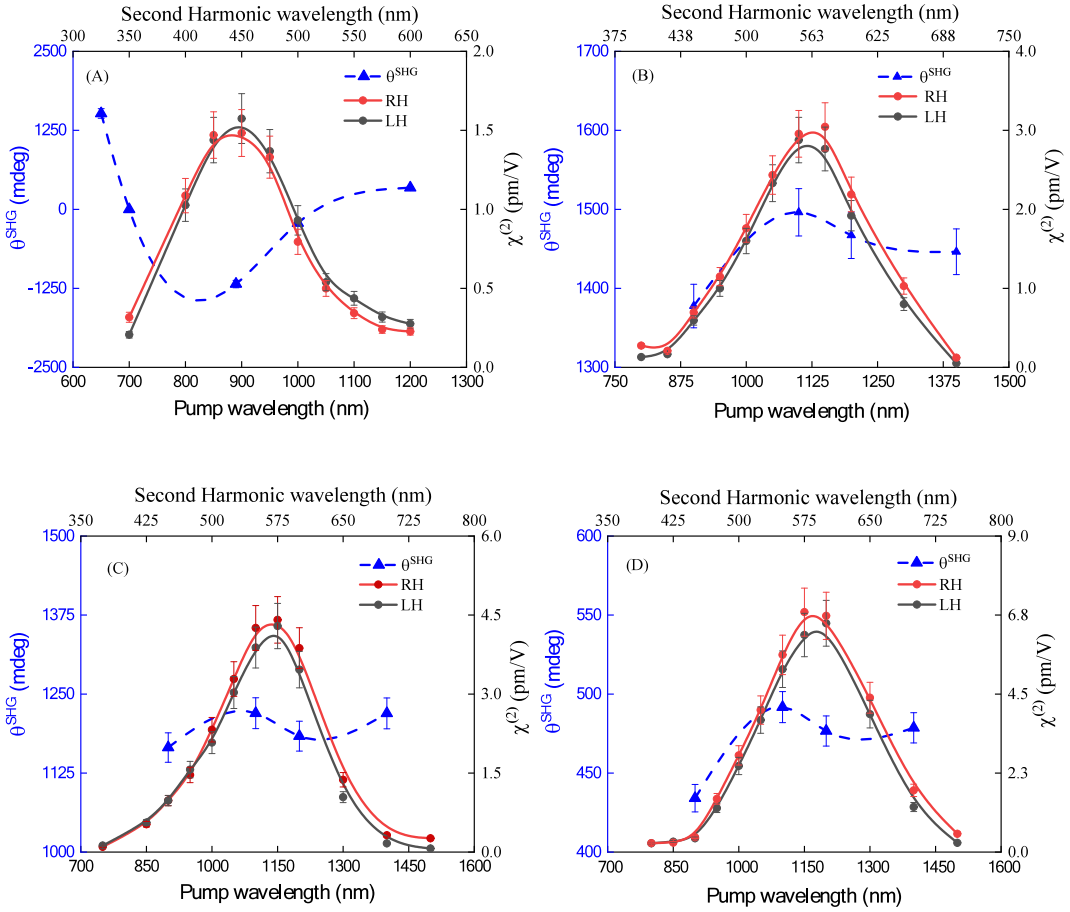

Figure 5. Graphs of OA-SHG dispersion for all samples in DMSO solution. The blue axis on the left represents the θ^{SHG} values, and the blue triangles are the experimental data. The dashed lines are just eye guides. The black axis at the right represents the $\chi^{(2)}$ values, where the red and black circles show the experimental data for RH and LH circular polarization. The solid lines are only present to guide the eye.

inversion of the $\chi^{(2)}$ is necessary to compensate for the phase difference of the wave vector ($\Delta\vec{k} \neq 0$), shifting one phase about the other along the coherence length l_c, which is defined as $l_c = \frac{\lambda}{4(n_{2\omega} - n_{\omega})}$; l_c generally has dimensions in units of tens of micrometers.[53]

To gain insights into the SHG signal, FDTD simulations[54] were performed. The structures were modeled as a 3D hollow cylinder inside a continuum medium with a refractive index of 1.48 (DMSO), excited by a Gaussian beam with a width of 8 μm and peak amplitude of 10^{10} V/m, focused on the structure. Given that the beam spot significantly exceeds the dimensions of the structure, the latter will experience an almost uniform electric field. To model the nonlinear optical response, the input $\chi^{(2)}$ values were obtained from the results of this work. At the same time, the linear refractive index dispersion was estimated by the Sellmeier model for similar polymers.[55,56] Then, in the simulated model n_{ω} = 1.48 and $n_{2\omega}$ = 2.24, the index phase-match condition is not established. Figure 4 illustrates the results obtained for the Pol D sample for a pumping wavelength at λ = 1200 nm. Similar results are found for other polymers. Figure 4a shows the simulation of the magnitude of the 2ω electric field as a function of the position of the sample. The color bar indicates the magnitude of the SHG signal. Figures 4b and 4c were elaborated to understand the additive effect of the magnitude at the 2ω field propagation throughout the structure. In Figure 4b, a longitudinal scan focused on the center of the structure was performed to analyze the 2ω electric field amplitude.

As can be seen, a progressive increase of 2ω in the first and second layers indicates a typical QPM process. Also, the 2ω signal is created with high amplitude in the first layer, while, in the hollow part, it decreases, and in the second layer, it is finally amplified. Figure 4c illustrates the integrated signal for each region indicated by the dashed lines in Figure 4b. There is an upward increase in the second harmonic electric field magnitude in the first layer, which remains constant in the hollow part. Therefore, it propagates again through the material, resulting in a considerable increase in the SHG signal via the QFM process. Furthermore, as the wavelength of the 2ω signal generated is approximately an integer of the difference in optical path length, it is suggested that there is the coupling of the field with the structure acting as a nanoresonator,[57−59] which, in turn, also acts as a mechanism for enhancement of SHG. Notably, no resonances were induced in the structures, likely due to their small diameter, which inhibits them from accommodating high-quality factor resonances for the wavelengths of interest.

Beyond the considerations of structure and shape in a supramolecular medium, chirality also plays a fundamental role in the SHG response. Some studies report that the NLO properties can be enhanced by chirality in supramolecular poled films.[34] In this medium, the magnetic-dipole interaction significantly contributes to the SHG values compared to the

https://doi.org/10.1021/acs.jpclett.5c02495
J. Phys. Chem. Lett. 2025, 16, 13007−13015

electric dipole one.[60−62] This phenomenon can be elucidated through the coupling between the backbone and chromophores, which leads to the inclusion of several nonzero tensor components in the second-order optical susceptibility.[63] To further evaluate the impact of chirality on SHG response, nonlinear optical activity measurements were performed on four samples in DMSO at low concentrations. The SHG technique was used with the insertion of a broadband one-quarter waveplate ($\lambda/4$) to control the change in polarization between linear, left (LH), and right-handed (RH) circular polarization before the incidence at the sample. The optical activity dispersion based on the SHG signal (OA-SHG) is illustrated in Figure 5 for all polymers in the DMSO solution. Details about the linear circular dichroism for these polymers can be found in ref 64. In all samples, a slight disparity is observed in the $\chi^{(2)}$ values between LH and RH circular polarizations, contingent upon the spectral position of the pump wavelength. One example of it is shown for Pol (A) in the SI. For 900 nm pump wavelength, Figure SI-5(a) displays the statistical measurements for all three polarization states. Besides, the ratio between the dispersion of $\chi^{(2)}$ values of circular and linear polarizations $\left(\frac{\chi^{(2)}_{\mathrm{LH/RH}}}{\chi^{(2)}_{\mathrm{Linear}}}\right)$ was $\sim\sqrt{2}/2$. Our results shows the difference between RH and LH circular polarization can ranges from 0.5% to 9%, as can be seen in some examples in Figure SI-5, which is undetectable by conventional SHG techniques.

Therefore, statistical measurements were performed for some pump wavelengths in the range from 625 nm to 1400 nm. The signal of $I(2\omega)$ was normalized by the intensity of the laser pump (reference signal (ω)) through a lock-in amplifier to avoid variations that do not come from the SHG. Thus, the SHG signal collected by a PMT was integrated for 1 s, and 60 averages were performed. The normalized $I(2\omega)$ measurements were taken for each sample at the wavelengths studied for each polarization. All the results were normalized by the linear polarization to verify the variation in SHG as a function of the right and left-handed polarizations. Thus, due to the stability of the pumping laser and the experimental system, the standard deviation between the measurements at a given polarization was between 0.5% and 1%.

Chiral nanomaterials may present intriguing features such as negative refractive index superchiral light and thermal realignment, which is interesting in chiral photonics applications.[63,65] For example, a flexible circularly polarized light (CPL) detector can be developed for potential applications such as security-enhanced, encrypted communications.[66] Despite this potential interest, gaining knowledge about the difference between RH and LH circular polarization plane angles is valuable. Thus, to quantify the angle of difference between the RH and LH circulars, based on the circular dichroism equation, we employed the following expression:[67]

$$\theta^{\mathrm{SHG}}\ (\mathrm{deg}) = \left(\frac{180}{\pi}\right)\left(\frac{\sqrt{\mathrm{I}(2\omega)^{\mathrm{SHG}}_{\mathrm{RH}}} - \sqrt{\mathrm{I}(2\omega)^{\mathrm{SHG}}_{\mathrm{LH}}}}{\sqrt{\mathrm{I}(2\omega)^{\mathrm{SHG}}_{\mathrm{RH}}} + \sqrt{\mathrm{I}(2\omega)^{\mathrm{SHG}}_{\mathrm{LH}}}}\right)^{-1}$$

where the terms $I(2\omega)^{\mathrm{SHG}}_{\mathrm{RH}}$ and $I(2\omega)^{\mathrm{SHG}}_{\mathrm{LH}}$ are the intensities of the SHG for the RH and LH circular pump polarization, respectively. An example of one of these measurements can be viewed in section S7 of the SI. For Pol B, Pol C, and Pol D, θ^{SHG} varies around 10% with the following order of magnitude: B > C > D. However, for Pol A, there is a significant variation in the amplitude and maximum at the θ^{SHG} values. The variation in amplitude is approximately 200%, and the difference between the intensities of the circular polarizations can reach around 9%. The inversion in θ^{SHG} values observed between 325 nm and 450 nm is associated with the Cotton effect in the structure of binaphthalene.[68−70] This effect is related to the combination of circular dichroism and optical activity in the chiral band, which results in a resonance enhancement effect due to the absorption of circularly polarized light. As in Pol A, the second harmonic of the first θ^{SHG} measurement is close to the chiral band; this effect occurs more intensely than in the other polymers. Thus, as the ellipticity value is higher for shorter wavelengths, Pol A has the negative Cotton effect, and the other samples with the opposite wavelength behavior are classified as a positive Cotton effect. Furthermore, with the characterization of this effect, it is possible to connect it to the linear circular dichroism results, in which the positive and negative Cotton effects are linked to the negative and positive linear CD values. Thus, when comparing the results reported in the literature by Koeckelberghs et al.[64] of the linear CD for the polymers studied here, as well as noting no changes in the spectral positions of the chirality as a function of the chromophores corroborated with the θ^{SHG} results.

Regarding the different θ^{SHG} values between the polymers, in addition to the Cotton effect, a possible explanation may be associated with the proximity of the binaphthalene absorption band to the chromophore absorption band, because chirality is related to the binaphthalene polymer chain. The binaphthalene absorption band is centered at the ultraviolet region (~350 nm)[43] and chromophore absorption bands of Pol A, Pol B, Pol C, and Pol D are centered, respectively, 450 nm, 554 nm, 572 and 605 nm, where the Pol A is closer than to other samples, being more susceptible to the influences of chirality at NLO response.

We embarked on a pioneering investigation, delving into the relationship between the structure and SHG dispersion of four novel chiral chromophore-functionalized polybinaphthalenes in a colloidal system. Initially, the dispersion of SHG was unveiled by the SHG technique employing linear polarization. These findings demonstrated a similar dispersion profile and notable disparity in the peak values. The DLS and AFM measurements showed that size and shape play a fundamental role, in addition to the strength of the EWG attached to the central polymer backbone. The rodlike/helical structure determined by AFM associated with the chromophore creates a periodic directional preference throughout the macrostructure for the $\chi^{(2)}$ coefficient, suggesting that the SHG origin is associated with a quasi-phase matching process, which is corroborated by FDTD simulations. Moreover, the SHG is enhanced by the 2PA process and by coupling the nonlinear electric field like a nanoresonator. The OA-SHG dispersion measurements distinguish between left-hand (LH) and right-hand (RH) circular polarization. Since chirality is intrinsic to the binaphthalene core, the angle of difference between the RH and LH circular values tends to decrease with a greater redshift in the absorption band of the chromophore. Therefore, such outcomes reveal key insights to lead new strategies for obtaining elevated SHG values at chiral supramolecular derivatives and provide remarkable applications related to the polarized resolved double-frequency conversion process, three-

https://doi.org/10.1021/acs.jpclett.5c02495
J. Phys. Chem. Lett. 2025, 16, 13007−13015

dimensional SHG microscopy at biological systems, and chiral photonics devices.

EXPERIMENTAL METHODS

The supramolecular second-order nonlinear dispersion values were determined by employing the external reference method (ERM), using a femtosecond spectral-resolved SHG technique that employed an optical parametric amplifier (Orpheus - Light Conversion) pumped by an amplified femtosecond laser system (Pharos - Light Conversion, 1030 nm, 190 fs, 7.5 kHz) as tunable laser excitation. The pNA dissolved at DMSO was used as a reference sample. More details can be found in ref 26. The $\chi^{(2)}$ values were calculated by normalizing the values of the first-order hyperpolarizability (β) by the volume of each structure. The measurements were performed over a range from 700 nm to 1500 nm with 50 nm intervals for linear and circular polarizations.

The DLS data were measured at concentrations of about 10 μM in pure DMSO in a quartz cuvette with an optical path of 1 cm. The films for AFM measurements were prepared using the spin-coating method on a silicon wafer. More details can be found in sections S4 and S5 of the SI.

The TDFD simulations were run for enough time for all the fields to decay and were analyzed in the frequency domain to obtain the field distribution at the pump and SHG frequencies. The simulation volume is surrounded by field monitors, which are used to accumulate and measure the total energy leaving the simulation domain. These field monitors are useful for analyzing SHG energy conversion. Additionally, to effectively truncate the simulations and prevent any unwanted reflections or artifacts, the simulation volume is enclosed by perfectly matched layers (PMLs). These PMLs are designed to absorb the electromagnetic fields exiting the simulation domain, ensuring that the boundaries do not interfere with the simulation results.

ASSOCIATED CONTENT

Supporting Information

The Supporting Information is available free of charge at https://pubs.acs.org/doi/10.1021/acs.jpclett.5c02495.

Absorbance spectra of all samples in dimethyl sulfoxide solution; example of quadratic dependence of the SH signal with the pump laser intensity; example of the linear dependence of the SHG quadratic coefficient with the concentration; description of the 2PA enhancement factor; description of the dynamic light scattering and atomic force microscopy measurements; relationship between $\chi^{(2)}$ and volume; example of the SHG signal as a function of the pump laser polarization (PDF)

Transparent Peer Review report available (PDF)

AUTHOR INFORMATION

Corresponding Author

Leonardo De Boni − *Instituto de Física de São Carlos, Universidade de São Paulo, São Carlos 13566-590 SP, Brazil;* orcid.org/0000-0002-1875-1852; Email: deboni@ifsc.usp.br

Authors

Carlos H. D. dos Santos − *Instituto de Física de São Carlos, Universidade de São Paulo, São Carlos 13566-590 SP, Brazil*

Marcelo G. Vivas − *Laboratório de Espectroscopia Óptica e Fotônica, Universidade Federal de Alfenas, Poços de Caldas 37701-840 MG, Brazil;* orcid.org/0000-0003-4777-1323

Filipe A. Couto − *Instituto de Física de São Carlos, Universidade de São Paulo, São Carlos 13566-590 SP, Brazil*

Guy Koeckelberghs − *Laboratory of Macromolecular and Physical Organic Chemistry, Katholieke Universiteit Leuven, B-3001 Heverlee, Belgium;* orcid.org/0000-0003-1412-8454

Cleber R. Mendonça − *Instituto de Física de São Carlos, Universidade de São Paulo, São Carlos 13566-590 SP, Brazil;* orcid.org/0000-0001-6672-2186

Complete contact information is available at: https://pubs.acs.org/10.1021/acs.jpclett.5c02495

Author Contributions

Carlos H.D. dos Santos conducted the experimental setup, performed SHG and structural measurements (DLS and AFM), analyzed the data, and wrote the paper. Marcelo G. Vivas contributed to data analysis, writing, and revision. Filipe A. Couto performed the SHG simulations. Guy Koeckelberghs was responsible for polymer synthesis. Cleber R. Mendonça contributed to writing and revising the paper. Leonardo De Boni conceived the idea, designed the SHG experimental setup, supervised the work, and contributed to writing and revision.

Funding

The Article Processing Charge for the publication of this research was funded by the Coordenacao de Aperfeicoamento de Pessoal de Nivel Superior (CAPES), Brazil (ROR identifier: 00x0ma614).

Notes

The authors declare no competing financial interest.

ACKNOWLEDGMENTS

The authors acknowledge financial support from the São Paulo Research Foundation (FAPESP), under Grant Nos. 2025/01908-3 and 2018/11283-7; FAPEMIG (Fundação de Amparo à Pesquisa do Estado de Minas Gerais), No. APQ-02101-23; Conselho Nacional de Desenvolvimento Científico e Tecnológico (CNPq); Coordenação de Aperfeiçoamento de Pessoal de Nível Superior, Brasil (CAPES), Código de Financiamento 001; the Air Force Office of Scientific Research (AFOSR), No. FA9550-23-1-0664; and the U.S. Army, No. W911NF2110362.

REFERENCES

(1) Koeckelberghs, G.; Sioncke, S.; Verbiest, T.; Persoons, A.; Samyn, C. Synthesis and properties of chiral helical chromophore-functionalised polybinaphthalenes for second-order nonlinear optical applications. *Polymer (Guildford)* **2003**, *44* (14), 3785−3794.

(2) Facchetti, A.; Annoni, E.; Beverina, L.; Morone, M.; Zhu, P.; Marks, T. J.; Pagani, G. A. Very large electro-optic responses in H-bonded heteroaromatic films grown by physical vapour deposition. *Nat. Mater.* **2004**, *3* (12), 910−917.

(3) Hilf, S.; Kilbinger, A. F. M. Functional end groups for polymers prepared using ring-opening metathesis polymerization. *Nat. Chem.* **2009**, *1* (7), 537−546.

(4) Nie, Z.; Kumacheva, E. Patterning surfaces with functional polymers. *Nat. Mater.* **2008**, *7* (4), 277−290.

(5) Antonietti, M. "Self-organization of functional polymers,". *Nat. Mater.* **2003**, *2* (1), 9−10.

(6) Zhu, B.; Qian, B.; Liu, Y.; Xu, C.; Liu, C.; Chen, Q.; Zhou, J.; Liu, X.; Qiu, J. A volumetric full-color display realized by frequency upconversion of a transparent composite incorporating dispersed nonlinear optical crystals. *NPG Asia Mater.* **2017**, *9* (6), No. e394.
(7) Abdelwahab, I.; Tilmann, B.; Wu, Y.; Giovanni, D.; Verzhbitskiy, I.; Zhu, M.; Berté, R.; Xuan, F.; Menezes, L. de S.; Eda, G.; Sum, T. C.; Quek, S. Y.; Maier, S. A.; Loh, K. P. Giant second-harmonic generation in ferroelectric $NbOI_2$. *Nat. Photonics* **2022**, *16* (9), 644−650.
(8) Hu, Y.-X.; Hao, X.; Xu, L.; Xie, X.; Xiong, B.; Hu, Z.; Sun, H.; Yin, G.-Q.; Li, X.; Peng, H.; Yang, H.-B. Construction of Supramolecular Liquid-Crystalline Metallacycles for Holographic Storage of Colored Images. *J. Am. Chem. Soc.* **2020**, *142* (13), 6285−6294.
(9) Chen, W.; Liu, T.; Zou, J.; Zhang, D.; Tse, M. K.; Tsang, S.; Luo, J.; Jen, A. K. Push-pull Heptamethines Near The Cyanine Limit Exhibiting Large Quadratic Electro-Optic Effect. *Adv. Mater.* **2024**, *36* (17), 2306089.
(10) Chen, S.; Li, K. F.; Li, G.; Cheah, K. W.; Zhang, S. Gigantic electric-field-induced second harmonic generation from an organic conjugated polymer enhanced by a band-edge effect. *Light Sci. Appl.* **2019**, *8* (1), 17.
(11) Baev, A.; Prasad, P. N. Chiral polymer photonics. *Opt Mater. Express* **2017**, *7* (7), 2432.
(12) Genet, C. Chiral Light-Chiral Matter Interactions: an Optical Force Perspective. *ACS Photonics* **2022**, *9* (2), 319−332.
(13) Billat, A.; Grassani, D.; Pfeiffer, M. H. P.; Kharitonov, S.; Kippenberg, T. J.; Brès, C.-S. Large second harmonic generation enhancement in Si_3N_4 waveguides by all-optically induced quasi-phase-matching. *Nat. Commun.* **2017**, *8* (1), 1016.
(14) Lin, J. T.; Hubbard, M. A.; Marks, T. J.; Lin, W.; Wong, G. K. Poled polymeric nonlinear optical materials. Exceptional second harmonic generation temporal stability of a chromophore-functionalized polyimide. *Chem. Mater.* **1992**, *4* (6), 1148−1150.
(15) Liu, M.; Zhang, L.; Wang, T. Supramolecular Chirality in Self-Assembled Systems. *Chem. Rev.* **2015**, *115* (15), 7304−7397.
(16) Sun, Q.; Wang, Y. A.; Li, L. S.; Wang, D.; Zhu, T.; Xu, J.; Yang, C.; Li, Y. Bright, multicoloured light-emitting diodes based on quantum dots. *Nat. Photonics* **2007**, *1* (12), 717−722.
(17) Akcora, P.; Liu, H.; Kumar, S. K.; Moll, J.; Li, Y.; Benicewicz, B. C.; Schadler, L. S.; Acehan, D.; Panagiotopoulos, A. Z.; Pryamitsyn, V.; Ganesan, V.; Ilavsky, J.; Thiyagarajan, P.; Colby, R. H.; Douglas, J. F. Anisotropic self-assembly of spherical polymer-grafted nanoparticles. *Nat. Mater.* **2009**, *8* (4), 354−359.
(18) Lan, X.; Liu, T.; Wang, Z.; Govorov, A. O.; Yan, H.; Liu, Y. DNA-Guided Plasmonic Helix with Switchable Chirality. *J. Am. Chem. Soc.* **2018**, *140* (37), 11763−11770.
(19) Hosono, N.; Gochomori, M.; Matsuda, R.; Sato, H.; Kitagawa, S. Metal-Organic Polyhedral Core as a Versatile Scaffold for Divergent and Convergent Star Polymer Synthesis. *J. Am. Chem. Soc.* **2016**, *138* (20), 6525−6531.
(20) Zheng, Y.; Li, S.; Weng, Z.; Gao, C. Hyperbranched polymers: advances from synthesis to applications. *Chem. Soc. Rev.* **2015**, *44* (12), 4091−4130.
(21) Wang, F.; Harper, A. W.; Lee, M. S.; Dalton, L. R.; Zhang, H.; Chen, A.; Steier, W. H.; Marder, S. R. Progress toward Device-Quality Second-Order NLO Materials: 3. Electrooptic Activity of Polymers Containing E, E, E -[4-(*N*,*N*-Dialkylamino)- phenyl]-pentadienylidene-3-phenyl-5-isoxazolone Chromophores. *Chem. Mater.* **1999**, *11* (9), 2285−2288.
(22) Wu, Y.; Yuan, Y.; Sorbelli, D.; Cheng, C.; Michalek, L.; Cheng, H.-W.; Jindal, V.; Zhang, S.; LeCroy, G.; Gomez, E. D.; et al. Tuning polymer-backbone coplanarity and conformational order to achieve high-performance printed all-polymer solar cells. *Nat. Commun.* **2024**, *15* (1), 2170.
(23) Clays, K.; Persoons, A. Hyper-Rayleigh scattering in solution. *Phys. Rev. Lett.* **1991**, *66* (23), 2980−2983.
(24) Campo, J.; Desmet, F.; Wenseleers, W.; Goovaerts, E. Highly sensitive setup for tunable wavelength hyper-Rayleigh scattering with parallel detection and calibration data for various solvents. *Opt. Express* **2009**, *17* (6), 4587.
(25) Campo, J.; Painelli, A.; Terenziani, F.; Van Regemorter, T.; Beljonne, D.; Goovaerts, E.; Wenseleers, W. First Hyperpolarizability Dispersion of the Octupolar Molecule Crystal Violet: Multiple Resonances and Vibrational and Solvation Effects. *J. Am. Chem. Soc.* **2010**, *132* (46), 16467−16478.
(26) dos Santos, C. H. D.; Zucolotto Cocca, L. H.; Pelosi, A. G.; Batista, V. F.; Pinto, D. C. G. A.; Faustino, M. A. F.; Vivas, M. G.; de Paula Siqueira, J.; Mendonça, C. R.; De Boni, L. Observation of the two-photon transition enhanced first hyperpolarizability spectra in cinnamaldehyde derivatives: A femtosecond regime study. *J. Chem. Phys.* **2023**, *158*, 214201.
(27) Verreault, D.; Moreno, K.; Merlet, É.; Adamietz, F.; Kauffmann, B.; Ferrand, Y.; Olivier, C.; Rodriguez, V. Hyper-Rayleigh Scattering as a New Chiroptical Method: Uncovering the Nonlinear Optical Activity of Aromatic Oligoamide Foldamers. *J. Am. Chem. Soc.* **2020**, *142* (1), 257−263.
(28) Joulaud, C.; Mugnier, Y.; Djanta, G.; Dubled, M.; Marty, J.-C.; Galez, C.; Wolf, J.-P.; Bonacina, L.; Le Dantec, R. Characterization of the nonlinear optical properties of nanocrystals by Hyper Rayleigh Scattering. *J. Nanobiotechnol.* **2013**, *11* (S1), S8.
(29) Chen, L.; Fu, P.; Wang, H.; Pan, M. Excited-State Intramolecular Proton Transfer (ESIPT) for Optical Sensing in Solid State. *Adv. Opt. Mater.* **2021**, *9* (23), 2001952.
(30) Kim, E.; Steinbrück, A.; Buscaglia, M. T.; Buscaglia, V.; Pertsch, T.; Grange, R. Second-Harmonic Generation of Single $BaTiO_3$ Nanoparticles down to 22 nm Diameter. *ACS Nano* **2013**, *7* (6), 5343−5349.
(31) Ohnoutek, L.; Cho, N. H.; Allen Murphy, A. W.; Kim, H.; Răsădean, D. M.; Pantoş, G. D.; Nam, K. T.; Valev, V. K. Single Nanoparticle Chiroptics in a Liquid: Optical Activity in Hyper-Rayleigh Scattering from Au Helicoids. *Nano Lett.* **2020**, *20* (8), 5792−5798.
(32) Clays, K. J.; Hendrickx, E.; Houbrechts, S.; Triest, M.; Verbiest, T.; Persoons, A. P.; Samyn, C. Characterization of polymeric nonlinear optical materials by hyper-Rayleigh scattering in solution. In *Nonlinear Optical Properties of Organic Materials VI*; Moehlmann, G. R., Ed.; Proceedings of the 1993 SPIE International Symposium on Optics, Imaging, and Instrumentation, Vol. *2025*; SPIE, 1993; p 182.
(33) Kauranen, M.; Verbiest, T.; Boutton, C.; Teerenstra, M. N.; Clays, K.; Schouten, A. J.; Nolte, R. J. M.; Persoons, A. Supramolecular Second-Order Nonlinearity of Polymers with Orientationally Correlated Chromophores. *Science* **1995**, *270* (5238), 966−969.
(34) Verbiest, T.; Van Elshocht, S.; Kauranen, M.; Hellemans, L.; Snauwaert, J.; Nuckolls, C.; Katz, T. J.; Persoons, A. Strong Enhancement of Nonlinear Optical Properties Through Supramolecular Chirality. *Science* **1998**, *282* (5390), 913−915.
(35) Guo, Z.; Li, J.; Liu, R.; Yang, Y.; Wang, C.; Zhu, X.; He, T. Spatially Correlated Chirality in Chiral Two-Dimensional Perovskites Revealed by Second-Harmonic-Generation Circular Dichroism Microscopy. *Nano Lett.* **2023**, *23* (16), 7434−7441.
(36) Cherifi-Hertel, S.; Bulou, H.; Hertel, R.; Taupier, G.; Dorkenoo, K. D.; Andreas, C.; Guyonnet, J.; Gaponenko, I.; Gallo, K.; Paruch, P. Non-Ising and chiral ferroelectric domain walls revealed by nonlinear optical microscopy. *Nat. Commun.* **2017**, *8* (1), 15768.
(37) Kriech, M. A.; Conboy, J. C. Imaging Chirality with Surface Second Harmonic Generation Microscopy. *J. Am. Chem. Soc.* **2005**, *127* (9), 2834−2835.
(38) Yan, P.; Millard, A. C.; Wei, M.; Loew, L. M. Unique Contrast Patterns from Resonance-Enhanced Chiral SHG of Cell Membranes. *J. Am. Chem. Soc.* **2006**, *128* (34), 11030−11031.
(39) Rodrigues, S. P.; Lan, S.; Kang, L.; Cui, Y.; Cai, W. Nonlinear Imaging and Spectroscopy of Chiral Metamaterials. *Adv. Mater.* **2014**, *26* (35), 6157−6162.
(40) Yin, F.; Liu, L.; Zhu, M.; Lv, J.; Guan, X.; Zhang, J.; Lin, N.; Fu, X.; Jia, Z.; Tao, X. Transparent Lead-Free Ferroelectric (K, Na)NbO_3 Single Crystal with Giant Second Harmonic Generation and Wide

https://doi.org/10.1021/acs.jpclett.5c02495
J. Phys. Chem. Lett. 2025, 16, 13007−13015

Mid-Infrared Transparency Window. *Adv. Opt. Mater.* **2022**, *10* (23), 1−7.
(41) Lodahl, P.; Mahmoodian, S.; Stobbe, S.; Rauschenbeutel, A.; Schneeweiss, P.; Volz, J.; Pichler, H.; Zoller, P. Chiral quantum optics. *Nature* **2017**, *541* (7638), 473−480.
(42) Yoo, S.; Park, Q.-H. Metamaterials and chiral sensing: a review of fundamentals and applications. *Nanophotonics* **2019**, *8* (2), 249−261.
(43) Koeckelberghs, G.; Vangheluwe, M.; Picard, I.; De Groof, L.; Verbiest, T.; Persoons, A.; Samyn, C. Synthesis and Properties of New Chiral Donor-Embedded Polybinaphthalenes for Nonlinear Optical Applications. *Macromolecules* **2004**, *37* (23), 8530−8537.
(44) Koeckelberghs, G.; Sioncke, S.; Verbiest, T.; Van Severen, I.; Picard, I.; Persoons, A.; Samyn, C. Synthesis and Properties of Chiral Chromophore-Functionalized Polybinaphthalenes for Nonlinear Optics: Influence of Chromophore Concentration. *Macromolecules* **2003**, *36* (26), 9736−9741.
(45) Silva, D. L.; Fonseca, R. D.; Vivas, M. G.; Ishow, E.; Canuto, S.; Mendonca, C. R.; De Boni, L. Experimental and theoretical investigation of the first-order hyperpolarizability of a class of triarylamine derivatives *J. Chem. Phys.* **2015** *142* (6), DOI: 10.1063/1.4906893.
(46) Vivas, M. G.; Silva, D. L.; Rodriguez, R. D. F.; Canuto, S.; Malinge, J.; Ishow, E.; Mendonca, C. R.; De Boni, L. Interpreting the First-Order Electronic Hyperpolarizability for a Series of Octupolar Push-Pull Triarylamine Molecules Containing Trifluoromethyl. *J. Phys. Chem. C* **2015**, *119* (22), 12589−12597.
(47) Sciuti, L. F.; Abegão, L. M. G.; dos Santos, C. H. D.; Zucolotto Cocca, L. H.; da Costa, R. G. M.; Limberger, J.; Misoguti, L.; Mendonça, C. R.; De Boni, L. Modeling the First-Order Molecular Hyperpolarizability Dispersion from Experimentally Obtained One- and Two-Photon Absorption. *J. Phys. Chem. A* **2022**, *126* (14), 2152−2159.
(48) dos Santos, C. H. D.; Zucolotto Cocca, L. H.; Pelosi, A. G.; Batista, V. F.; Pinto, D. C. G. A.; Faustino, M. A. F.; Vivas, M. G.; de Paula Siqueira, J.; Mendonça, C. R.; De Boni, L. Observation of the two-photon transition enhanced first hyperpolarizability spectra in cinnamaldehyde derivatives: A femtosecond regime study *J. Chem. Phys.* **2023**, *158* (21), DOI: 10.1063/5.0151622.
(49) Babick, F. Dynamic light scattering (DLS). In *Characterization of Nanoparticles*; Elsevier, 2020; pp 137−172.
(50) Chen, J.; Žídek, K.; Chábera, P.; Liu, D.; Cheng, P.; Nuuttila, L.; Al-Marri, M. J.; Lehtivuori, H.; Messing, M. E.; Han, K.; Zheng, K.; Pullerits, T. Size- and Wavelength-Dependent Two-Photon Absorption Cross-Section of $CsPbBr_3$ Perovskite Quantum Dots. *J. Phys. Chem. Lett.* **2017**, *8* (10), 2316−2321.
(51) Alo, A.; Barros, L. W. T.; Nagamine, G.; Lemus, J. C.; Planelles, J.; Movilla, J. L.; Climente, J. I.; Lee, H. J.; Bae, W. K.; Padilha, L. A. Beyond Universal Volume Scaling: Tailoring Two-Photon Absorption in Nanomaterials by Heterostructure Design. *Nano Lett.* **2023**, *23* (15), 7180−7187.
(52) Van Elshocht, S.; Busson, B.; Verbiest, T.; Kauranen, M.; Snauwaert, J.; Hellemans, L.; Persoons, A.; Nuckolls, C.; Katz, T. J. Enhancement of Nonlinear Optical Properties Through Supramolecular Chirality. *MRS Proc.* **1999**, *561*, 15.
(53) Fejer, M. M.; Magel, G. A.; Jundt, D. H.; Byer, R. L. Quasi-phase-matched second harmonic generation: tuning and tolerances. *IEEE J. Quantum Electron.* **1992**, *28* (11), 2631−2654.
(54) Oskooi, A. F.; Roundy, D.; Ibanescu, M.; Bermel, P.; Joannopoulos, J. D.; Johnson, S. G. Meep: A flexible free-software package for electromagnetic simulations by the FDTD method. *Comput. Phys. Commun.* **2010**, *181* (3), 687−702.
(55) Shockravi, A.; Javadi, A.; Abouzari-Lotf, E. Binaphthyl-based macromolecules: a review. *RSC Adv.* **2013**, *3* (19), 6717.
(56) Javadi, A.; Najjar, Z.; Bahadori, S.; Vatanpour, V.; Malek, A.; Abouzari-Lotf, E.; Shockravi, A. High refractive index and low-birefringence polyamides containing thiazole and naphthalene units. *RSC Adv.* **2015**, *5* (111), 91670−91682.
(57) Frigenti, G.; Farnesi, D.; Pelli, S.; Nunzi Conti, G.; Soria, S. Nonlinear effects in optical micro- and nanoresonators. In *Advances in Nonlinear Photonics*; Elsevier, 2023; pp 439−466.
(58) Yamamoto, Y.; Yamagishi, H.; Huang, J.-S.; Lorke, A. Molecular and Supramolecular Designs of Organic/Polymeric Micro-photoemitters for Advanced Optical and Laser Applications. *Acc. Chem. Res.* **2023**, *56* (12), 1469−1481.
(59) Tulek, A.; Polson, R. C.; Vardeny, Z. V. Naturally occurring resonators in random lasing of π-conjugated polymer films. *Nat. Phys.* **2010**, *6* (4), 303−310.
(60) Govorov, A. O.; Fan, Z.; Hernandez, P.; Slocik, J. M.; Naik, R. R. Theory of Circular Dichroism of Nanomaterials Comprising Chiral Molecules and Nanocrystals: Plasmon Enhancement, Dipole Interactions, and Dielectric Effects. *Nano Lett.* **2010**, *10* (4), 1374−1382.
(61) Sato, S.; Yoshii, A.; Takahashi, S.; Furumi, S.; Takeuchi, M.; Isobe, H. Chiral intertwined spirals and magnetic transition dipole moments dictated by cylinder helicity. *Proc. Natl. Acad. Sci. U. S. A.* **2017**, *114* (50), 13097−13101.
(62) Lucassen, J.; Meijer, M. J.; Kurnosikov, O.; Swagten, H. J. M.; Koopmans, B.; Lavrijsen, R.; Kloodt-Twesten, F.; Frömter, R.; Duine, R. A. Tuning Magnetic Chirality by Dipolar Interactions. *Phys. Rev. Lett.* **2019**, *123* (15), 157201.
(63) Sioncke, S.; Verbiest, T.; Persoons, A. Second-order nonlinear optical properties of chiral materials. *Mater. Sci. Eng.: R.* **2003**, *42* (5−6), 115−155.
(64) Koeckelberghs, G.; Sioncke, S.; Verbiest, T.; Persoons, A.; Samyn, C. Synthesis and Properties of Chiral Donor-Embedded Polybinaphthalenes for Nonlinear Optical Applications. *Chem. Mater.* **2003**, *15* (15), 2870−2872.
(65) Nowacki, B.; Oh, H.; Zanlorenzi, C.; Jee, H.; Baev, A.; Prasad, P. N.; Akcelrud, L. Design and Synthesis of Polymers for Chiral Photonics. *Macromolecules* **2013**, *46* (18), 7158−7165.
(66) Gao, K.; Kim, S.; Zhao, W.; Ye, X.; Wang, P.; Liu, L.; Ahn, J.; Zhuo, H.; Li, Z.; Wang, Z.; et al. High-performance flexible circularly polarized light photodetectors based on chiral n-type naphthalenediimide-bithiophene polymers. *Npj Flexible Electron.* **2025**, *9* (1), 83.
(67) Collins, J. T.; Rusimova, K. R.; Hooper, D. C.; Jeong, H.-H.; Ohnoutek, L.; Pradaux-Caggiano, F.; Verbiest, T.; Carbery, D. R.; Fischer, P.; Valev, V. K. First Observation of Optical Activity in Hyper-Rayleigh Scattering. *Phys. Rev. X* **2019**, *9* (1), 011024.
(68) Nitti, A.; Pasini, D. Aggregation-Induced Circularly Polarized Luminescence: Chiral Organic Materials for Emerging Optical Technologies *Adv. Mater.* **2020**, *32* (41), DOI: 10.1002/adma.201908021.
(69) Zhang, X.; Xu, Z.; Zhang, Y.; Quan, Y.; Cheng, Y. Controllable Circularly Polarized Electroluminescence Performance Improved by the Dihedral Angle of Chiral-Bridged Binaphthyl-Type Dopant Inducers. *ACS Appl. Mater. Interfaces* **2021**, *13* (46), 55420−55427.
(70) Cornelis, D.; Franz, E.; Asselberghs, I.; Clays, K.; Verbiest, T.; Koeckelberghs, G. Interchromophoric Interactions in Chiral X-type π-Conjugated Oligomers: A Linear and Nonlinear Optical Study. *J. Am. Chem. Soc.* **2011**, *133* (5), 1317−1327.